



Continuous vs. discrete fractional Fourier transforms

Natig M. Atakishiyev^a, Luis Edgar Vicent^b, Kurt Bernardo Wolf^{c, *}

^a*Instituto de Matemáticas, Universidad Nacional Autónoma de México, Mexico*

^b*Facultad de Ciencias, Universidad Autónoma del Estado de Morelos, Mexico*

^c*Centro de Ciencias Físicas, Universidad Nacional Autónoma de México, Apartado Postal 48-3, Cuernavaca, Morelos 62251, México*

Received 9 December 1998

Abstract

We compare the finite Fourier (-exponential) and Fourier–Krivchuk transforms; both are discrete, finite versions of the Fourier integral transform. The latter is a canonical transform whose fractionalization is well defined. We examine the harmonic oscillator wavefunctions and their finite counterparts: Mehta’s basis functions and the Kravchuk functions. The fractionalized Fourier–Krivchuk transform was proposed in *J. Opt. Soc. Amer. A* (14 (1997) 1467–1477) and is here subject of numerical analysis. In particular, we follow the harmonic motions of coherent states within a finite, discrete optical model of a shallow multimodal waveguide. © 1999 Elsevier Science B.V. All rights reserved.

MSC: 33C45; 42C99; 44A55; 78A99

Keywords: Fractional Fourier transform; Kravchuk (Krawtchouk) polynomial; Waveguide; Coherent state

1. Introduction: canonical fractional Fourier transforms

The Fourier transform is a unitary operator $\mathcal{F} : \mathcal{L}^2(\mathfrak{R}) \mapsto \mathcal{L}^2(\mathfrak{R})$ that maps (the Hilbert spaces of Lebesgue) square-integrable functions on square-integrable ones, and is represented on these functions $\psi(q)$ by the well-known integral [32]

$$(\mathcal{F} \psi)(p) = \tilde{\psi}(p) = \frac{1}{\sqrt{2\pi}} \int_{\mathfrak{R}} dq e^{-ipq} \psi(q). \quad (1)$$

Relevant properties are that the square $(\mathcal{F}^2 \psi)(q) = \psi(-q)$ is the inversion operator, and that its fourth power, $(\mathcal{F}^4 \psi)(q) = \psi(q)$, is the identity; hence $\mathcal{F}^3 = \mathcal{F}^{-1} = \mathcal{F}^\dagger$.

* Corresponding author. Fax: +5273 17-3388.

E-mail address: bwolf@ce.ifisicam.unam.mx (K.B. Wolf)

On infinitely differentiable functions of fast decrease in $q \in \mathfrak{R}$, the Fourier operator \mathcal{F} can be written in hyperdifferential form [33, Eq. (7.197)]:

$$\mathcal{F} = e^{i\pi/4} \exp \left[\frac{-i\pi}{4} \left(-\frac{d^2}{dq^2} + q^2 \right) \right], \quad (2)$$

where we recognize the Hamiltonian operator of harmonic oscillator in quantum mechanics. From this follows that the oscillator eigenfunctions, given by Hermite functions $\Psi_n(q)$ with energy eigenvalues $\sim (n + \frac{1}{2})$, $n = 0, 1, 2, \dots$, will also be eigenfunctions of the Fourier operator, viz.,

$$(\mathcal{F} \Psi_n)(q) = e^{-i\pi n/2} \Psi_n(q), \quad (3)$$

$$\Psi_n(q) = e^{-q^2/2} H_n(q) / \sqrt{2^n n! \sqrt{\pi}}. \quad (4)$$

The operator \mathcal{F} thus generates a cyclic group of order 4.

The embedding of the Fourier transform into a continuous group of unitary transformations on $\mathcal{L}^2(\mathfrak{R})$ so that \mathcal{F}^α be defined for $\alpha \in \mathfrak{R} \bmod 4$ ($\alpha \equiv \alpha + 4$), with the property that $\mathcal{F}^\alpha \mathcal{F}^\beta = \mathcal{F}^{\alpha+\beta}$, was made by Condon in [11].¹ He found the integral kernel from the requirement of the rotational covariance of the Schrödinger position and momentum operators $Q = q$, $P = -id/dq$, by solving a partial differential equation, and adapting the normalization and phase to the desired group property. His result is

$$F^\alpha(q, q') = \frac{e^{-i\delta}}{\sqrt{2\pi \sin \frac{\pi}{2}\alpha}} \exp \left[\frac{i}{2 \sin \frac{\pi}{2}\alpha} (q'^2 \cos \frac{\pi}{2}\alpha - 2q'q + q^2 \cos \frac{\pi}{2}\alpha) \right], \quad (5)$$

where $\delta = \frac{1}{4}\pi$ for $\frac{\pi}{2}\alpha$ in the first two quadrants and $\delta = \frac{3}{4}\pi$ in its third or fourth quadrant.

Moshinsky and Quesne [22,23] employed the method of covariance to investigate general linear (symplectic) transformations $\text{Sp}(2, \mathfrak{R})$, given by a 2×2 matrix \mathbf{M} , between the two Schrödinger operators on $\mathcal{L}^2(\mathfrak{R})$, namely,

$$\mathcal{C}(\mathbf{M}) : \begin{pmatrix} Q \\ P \end{pmatrix} = \mathbf{M}^{-1} \begin{pmatrix} Q \\ P \end{pmatrix}, \quad \mathbf{M} = \begin{pmatrix} a & b \\ c & d \end{pmatrix}, \quad \det \mathbf{M} = 1, \quad (6)$$

$$[\mathcal{C}(\mathbf{M})\psi](q) = \int_{\mathfrak{R}} dq' C_M(q, q') \psi(q'), \quad (7)$$

$$C_M(q, q') = \frac{e^{-i\pi/4}}{\sqrt{2\pi b}} \exp \left[\frac{i}{2b} (aq'^2 - 2q'q + dq^2) \right]. \quad (8)$$

In particular, the fractional Fourier transform subgroup is found for

$$\mathcal{F}^\alpha = e^{i\pi\alpha/4} \mathcal{C}(\mathbf{F}^\alpha), \quad \mathbf{F}^\alpha = \begin{pmatrix} \cos \frac{1}{2}\pi\alpha & \sin \frac{1}{2}\pi\alpha \\ -\sin \frac{1}{2}\pi\alpha & \cos \frac{1}{2}\pi\alpha \end{pmatrix}, \quad (9)$$

¹ Note that this author uses the kernel $e^{i\rho q}$ instead of the more common $e^{-i\rho q}$ that we use here.

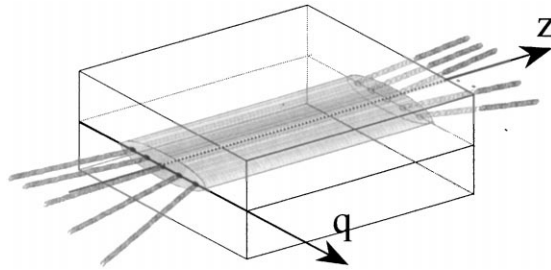


Fig. 1. Shallow multimodal waveguide, with a finite number of coherent input light-emitting devices and of output field sensors, performs the fractional Fourier–Kravchuk transform.

where the Fourier transform (1) corresponds to $\alpha = 1$. The integral kernel (8) for the matrix entries of (9) is (5). The phases are nontrivial and have to be treated carefully because the canonical transform operators $\mathcal{C}(M)$ actually represent the double cover of the group $Sp(2, \mathfrak{R})$ of 2×2 real symplectic matrices M , called the *metaplectic* group $Mp(2, \mathfrak{R})$. In what follows we shall work with Gaussians which, as we shall see, give meaning to the kernel (8) on a region of the complex plane of the parameters, and resolve the apparent phase ambiguities.

Another approach to fractionalization of a canonical transform into a one-parameter subgroup, uses the generating function of the eigenbasis of the subgroup generator, such as (3). There are three nonequivalent such subgroups in $Sp(2, \mathfrak{R})$, from which the integral transform kernel can be computed [33, Eqs. (9.88)]. For the cyclic subgroup where the Fourier transform lies, in 1980 Namias [24] reported that

$$C_{F^\alpha}(q, q') = e^{-i\pi\alpha/4} \sum_{n=0}^{\infty} \Psi_n(q) e^{-i\pi n\alpha/2} \Psi_n(q'). \tag{10}$$

This form shows the non-uniqueness of the fractionalization process: the n th summand in (10) is multiplied by the phase of exponent $-i\frac{\pi}{2}(n + \frac{1}{2})\alpha$ in accordance with (3); but if this were replaced by $-i\frac{\pi}{2}[v(n) + \frac{1}{2}]\alpha$, where $v(n)$ is any function on the integers such that $v(n) \equiv n \pmod{4}$, the Fourier transform will be regained for $\alpha = 1$, but with different fractionalizations. Only the phase in (10) yields the canonical transform (9) and hyperdifferential form (2).

Fractional Fourier transforms were recently introduced into paraxial wave optics by Lohmann et al. [21,27] within the model of two-dimensional waveguides of arbitrary length, and realized by lens-and-displacement optical arrangements. If the processing of data is to be performed through miniaturized multimodal waveguides, however, it is of interest to replace the infinite real line of the Fourier transform integration by a finite interval that reflects better the physical limitations of shallow waveguides; and to adapt the mathematical formalism to handle the input and output wavefields as data values on a finite number of discrete sensors, in a configuration such as that suggested in Fig. 1.

This article compares the ‘continuous’ fractional Fourier integral transform surveyed above with discrete, finite versions of this transform. The first that comes to mind is the well-known finite Fourier transform, that we call here *Fourier-exponential* transform because it is produced by a matrix with exponential-phase elements; one of its fractionalizations is surveyed in Section 2, together with its action on Gaussian functions. Section 3 is devoted to a résumé of the fractional Fourier–Kravchuk transform introduced in Ref. [6], that is based on the Kravchuk functions. These are the closest

counterpart of the ‘continuous’ Hermite functions in that they satisfy a *difference* equation over a finite number of points, which is a discrete, finite version of the harmonic oscillator Schrödinger equation.

The canonical fractional Fourier transform operator (9) of power α governs the evolution of a quantum harmonic oscillator, and the kernel (5) is its Green function for time $\tau = \frac{1}{2}\pi\alpha$ [2]. The motion of Gaussian functions in this environment can be found by realizing that these are *complex* canonical transform kernels [33, Eqs. (9.84) and (9.85)]:

$$G_w(q - q_0) = \frac{1}{\sqrt{2\pi w}} \exp\left[-\frac{(q - q_0)^2}{2w}\right] = \left[\mathcal{C} \begin{pmatrix} 1 & e^{-i\pi/2} w \\ 0 & 1 \end{pmatrix} \delta_{q_0} \right] (q), \quad (11)$$

where $\text{Re } w > 0$ is the width, q_0 is the center, and $\delta_{q_0}(q) = \delta(q - q_0)$ is the Dirac δ . Because canonical transforms compose as their matrices do, it follows that the fractional Fourier transform of a Gaussian is

$$\begin{aligned} G_w(q - q_0; \alpha) &= (\mathcal{F}^\alpha G_w(\circ - q_0))(q) \\ &= \left[\mathcal{C} \begin{pmatrix} \cos \frac{1}{2}\pi\alpha & -\sin \frac{1}{2}\pi\alpha \\ \sin \frac{1}{2}\pi\alpha & \cos \frac{1}{2}\pi\alpha \end{pmatrix} G_w(\circ - q_0) \right] (q) \\ &= \left[\mathcal{C} \begin{pmatrix} \cos \frac{1}{2}\pi\alpha & -\sin \frac{1}{2}\pi\alpha \\ \sin \frac{1}{2}\pi\alpha & \cos \frac{1}{2}\pi\alpha \end{pmatrix} \mathcal{C} \begin{pmatrix} 1 & e^{-i\pi/2} w \\ 0 & 1 \end{pmatrix} \delta_{q_0} \right] (q) \\ &= \left[\mathcal{C} \begin{pmatrix} \cos \frac{1}{2}\pi\alpha & -\sin \frac{1}{2}\pi\alpha - iw \cos \frac{1}{2}\pi\alpha \\ \sin \frac{1}{2}\pi\alpha & \cos \frac{1}{2}\pi\alpha - iw \sin \frac{1}{2}\pi\alpha \end{pmatrix} \delta_{q_0} \right] (q). \end{aligned} \quad (12)$$

The 1–2 matrix element b in the kernel (8), which appears under a square root, has now a well-defined phase in the third and fourth quadrants.

In Fig. 2 we show the fractional Fourier transform of a Gaussian of width $w = 1$ during the quarter-cycle between $\alpha = 0$ and $\alpha = 1$. This Gaussian is a coherent state for the quantum harmonic oscillator, so its motion should be familiar and serve as a useful comparison with any discrete version of the fractional Fourier transform that purports to describe a scalar field in a waveguide. Section 4 focuses on the finite oscillator coherent states; the figures show that the motion of these wavefields along the ‘finite’ waveguide are already indistinguishable from the continuous case for moderately large number of sensor points. The comparison between the two discrete transforms of Sections 2 and 3 is further commented in the closing Section 5, which adds some remarks on the fractionalization and discretization processes. Appendix contain a digest of the Feinsilver–Schott Kravchuk-transform algorithm.

2. Fractional Fourier-exponential transform

The discrete Fourier transform is the map of an $M \times M$ matrix \mathbf{E} on vectors $\mathbf{f} = \|f_m\|$ in \mathfrak{R}^M . Its elements involve the M th roots of unity, and are

$$\mathbf{E} = \|E_{m,n}\| = \frac{1}{\sqrt{M}} \|\omega_M^{-mn}\|, \quad \omega_M = e^{2\pi i/M}. \quad (13)$$

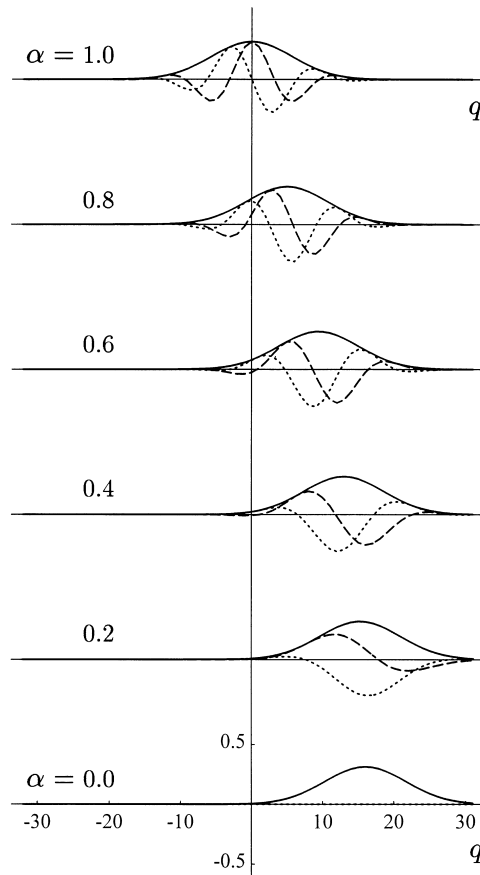


Fig. 2. Gaussian coherent state under fractional Fourier transformation by powers (from bottom to top) $\alpha = 0, 0.2, \dots, 1$. The initial function is a displaced Gaussian of appropriate width (chosen so that it does not ‘breathe’); the motion of its center is harmonic (a quarter-cycle is shown). We indicate by $---$ the real part, by \dots the imaginary part, and by $—$ the modulus.

It is symmetric ($\mathbf{E} = \mathbf{E}^T$), of unit determinant, unitary ($\mathbf{E}^\dagger = \mathbf{E}^{-1} = \mathbf{E}^* \in \text{SU}(M)$), its rows and columns are periodic modulo M (i.e., $E_{m,n} = E_{m+M,n} = E_{m,n+M}$); its square is the inversion matrix: $(\mathbf{E}^2 \mathbf{f})_m = f_{M-m}$, and its fourth power is thus unity: $\mathbf{E}^4 = \mathbf{1}$. Since other ‘Fourier’ matrices will appear in the text, we characterize this one by calling it the *Fourier-exponential* matrix, and count $m, n = 0, 1, 2, \dots, M - 1$.

To fractionalize the Fourier-exponential matrix (13) into a one-parameter group of unitary matrices is not a unique proposition, because its spectrum is degenerate for $M \geq 4$. It consists of four points on the unit circle: $1, -1, i$, and $-i$. For dimension M , the four eigenvalues appear with multiplicities $[\frac{1}{4}(M + 4)]$, $[\frac{1}{4}(M + 2)]$, $[\frac{1}{4}(M - 1)]$ and $[\frac{1}{4}(M + 1)]$, respectively $[1, 12, 15, 18-20, 31, 34]$, where the brackets $[\mu]$ indicate the largest integer not greater than μ . An interesting set of eigenvectors found by Mehta [20] is an infinite sequence of Hermite functions (4) displaced by 2π ; where the sum is

evaluated on a linear, periodic lattice of M points spaced by $2\pi/M$:

$$\Upsilon_n^M(m) = \sum_{j=-\infty}^{\infty} \Psi_n \left(\sqrt{\frac{2\pi}{M}}(m + jM) \right), \quad \begin{array}{l} n = 0, 1, 2, \dots, \\ m = 0, 1, \dots, M - 1. \end{array} \quad (14)$$

For uniformity in the figures it will be convenient to consider the m 's in a symmetric interval around the origin when M is odd, from $-\frac{1}{2}(M-1)$ to $\frac{1}{2}(M-1)$; for M even, m from $-\frac{1}{2}M$ to $\frac{1}{2}M-1$. The vectors (14) satisfy

$$E\Upsilon_n^M = (-i)^n \Upsilon_n^M, \quad n = 0, 1, 2, \dots \quad (15)$$

Two of these eigenvectors, Υ_n^M and $\Upsilon_{n'}^M$, are orthogonal when $n \neq n' \pmod{4}$. But since there is an infinity of vectors (14), a linearly independent, finite subset is found, for M even: $n \in \mathcal{M} = \{0, 1, \dots, M-1\}$. For M odd, Ref. [20] uses $n \in \mathcal{M} = \{0, 1, \dots, M-2, M\}$.

Once a basis $\{\Upsilon_n^M\}_{n \in \mathcal{M}}$ has been chosen and its dual basis $\{\Upsilon_n^{M*}\}_{n \in \mathcal{M}}$ is known, a fractional Fourier matrix can be defined using (15) in a generating function, with phases given by a function $v(n)$ of the integers on the integers as in (10),

$$E^\alpha = \|E_{m,m'}^\alpha\|, \quad E_{m,m'}^\alpha = \sum_{n \in \mathcal{M}} \Upsilon_n^{M*}(m) e^{-i(\pi/2)v(n)\alpha} \Upsilon_n^M(m'). \quad (16)$$

By choosing different $v(n)$'s we place the $E^\alpha \in \text{SU}(M)$ on different one-parameter subgroups joining (13) to the origin $E^0 = \mathbf{1}$.

Mehta's Fourier eigenbasis (14) shows also how the continuous and discrete fractional Fourier transforms will differ. The ground state Υ_0^M is 'almost' a Gaussian, because its neighboring copies are 2π widths to each side and contribute little to the Gaussian in the main interval. For higher- n states however, resemblances with the harmonic oscillator wavefunctions will end. Moreover, there does not seem to be any closed formula for the matrix elements $E_{m,m'}^\alpha$, nor a simple algorithm for the transformation of the data points $\{f_m\}_{m=0}^{M-1}$ under the discrete Fourier transform fractionalized in this way.

Before presenting the obvious modulo-4 fractionalization of the Fourier-exponential matrix, we must cite other approaches to discretization of the Fourier transform in bases that involve harmonic oscillator functions. Thus, Belingeri and Ricci [7,8] note that an (infinite) orthogonal polynomial system $\{P_n(x)\}_{n=0}^\infty$ has finite sub-bases: the zeros of $P_{M+1}(x)$, – call them x_0, x_1, \dots, x_M – provide the discrete orthogonality set for the basis of polynomials $\{P_n(x)\}_{n=0}^M$. The discrete Fourier transform (13) is used for the Hermite case developed in Ref. [7,8], allowing the Fast Fourier Transform algorithm to perform part of the computational load. If we interpret the points of orthogonality $\{x_m\}_{m=0}^M$ as the coordinates of a line of field sensors in a two-dimensional multimodal waveguide, their spacing will be that of the zeros of the Hermite function $\Psi_{M+1}(x)$, a set symmetric about the origin, bounded by $\frac{1}{2}M$, and slightly crowded towards the center of the interval.

Another approach to fractionalization of the Fourier transform seen as a phase-space rotation, is provided by the work of Hakioglu [16] on the Heisenberg–Weyl twist-product on a *torus*, with the definition of a proper Wigner function on the spaces of action and angle, and phase and number. The formalism extends to q -algebras, which apply elegantly to generalize the mechanical model of a Brillouin lattice of masses and springs [33, Chapters 1 and 2]. However, the topology of the torus

would seem to obstruct the fractionalization of the Fourier transform as a rotation of phase space, because the ‘coordinate axes’ are two inequivalent circles. Also note the work of Santhanam [28,29] on the number operator eigenbasis.

The requirements for the fractionalization of the finite Fourier-exponential transform (13) can be met in a rather simple way for any idempotent matrix or operator F such that $F^K = 1$, in particular the $M \times M$ Fourier matrix E for $K = 4$. A linear combination of F and its powers provides a basis for a complex, closed field where we can write real powers α of F modulo 4, as

$$F^\alpha = \varphi_1(\alpha)F + \varphi_2(\alpha)F^2 + \varphi_3(\alpha)F^3 + \varphi_4(\alpha)1. \tag{17}$$

To find the coefficients $\varphi_k(\alpha)$ we can use any faithful realization of F , in particular that of diagonal matrices $\text{diag}(\omega, \omega^2, \omega^3, 1)$, where $\omega = \omega_4 = e^{i\pi/2} = i$ is a fourth root of unity. The simplest solution in this realization is $F^\alpha = \text{diag}(\omega^\alpha, \omega^{2\alpha}, \omega^{3\alpha}, \omega^{4\alpha})$, which allows us to write (17) as a four-dimensional vector equation for $\boldsymbol{\varphi} = (\varphi_k(\alpha))_{k=1}^4$ with elements of the 4×4 Fourier-exponential matrix (13). This is easily inverted to

$$\begin{aligned} \begin{pmatrix} \varphi_1(\alpha) \\ \varphi_2(\alpha) \\ \varphi_3(\alpha) \\ \varphi_4(\alpha) \end{pmatrix} &= \frac{1}{4} \begin{pmatrix} -i & -1 & i & 1 \\ -1 & 1 & -1 & 1 \\ i & -1 & i & 1 \\ 1 & 1 & 1 & 1 \end{pmatrix} \begin{pmatrix} \omega^\alpha \\ \omega^{2\alpha} \\ \omega^{3\alpha} \\ \omega^{4\alpha} \end{pmatrix} \\ &= e^{5\pi\alpha/4} \begin{pmatrix} \frac{-1+i}{2} \sin \frac{1}{2}\pi\alpha (\cos \frac{1}{4}\pi\alpha + \sin \frac{1}{4}\pi\alpha) \\ i \cos \frac{1}{2}\pi\alpha \sin \frac{1}{4}\pi\alpha \\ \frac{1+i}{2} \sin \frac{1}{2}\pi\alpha (\cos \frac{1}{4}\pi\alpha - \sin \frac{1}{4}\pi\alpha) \\ \cos \frac{1}{2}\pi\alpha \cos \frac{1}{4}\pi\alpha \end{pmatrix}, \end{aligned} \tag{18}$$

$$\text{i.e., } \varphi_k(\alpha) = \frac{1}{4} e^{i5\pi(\alpha-k)/4} \frac{\sin \pi(\alpha - k)}{\sin \frac{1}{4}\pi(\alpha - k)}. \tag{19}$$

This solution yields the composition property $F^{\alpha_1}F^{\alpha_2} = F^{\alpha_1+\alpha_2}$ in all representations for F , in particular the $M \times M$ Fourier-exponential matrix E (13). The E^α thus constructed will be unitary because the coefficients in (18) satisfy $\varphi_1(\alpha) = \varphi_3(-\alpha)^*$, $\varphi_2(\alpha) = \varphi_2(-\alpha)^*$, and $\varphi_4(\alpha) = \varphi_4(-\alpha)$.

Compare now the canonical fractional Fourier transform (9) of a Gaussian, given by Eq. (12) and shown in Fig. 2, with the discrete version (17) of the Fourier-exponential transform in Fig. 3. As suggested by (14), we choose for input data the vector with the M values of a displaced Gaussian, at points around the origin spaced by $2\pi/M$. From the discussion on Mehta’s basis, we know that the discrete Fourier transform of a Gaussian will be approximately Gaussian, with phase oscillation due to the initial displacement. The quarter-cycle shown in Fig. 3 however, evinces that the harmonic motion of the Gaussian is *not* well reproduced. This fractionalization, for all α except the integers, contains always the original function and its mirror image, its Fourier transform and the inverse. We conclude that the fractional Fourier-exponential discrete transform (17)–(19) is *not* an appropriate model for harmonic motion.

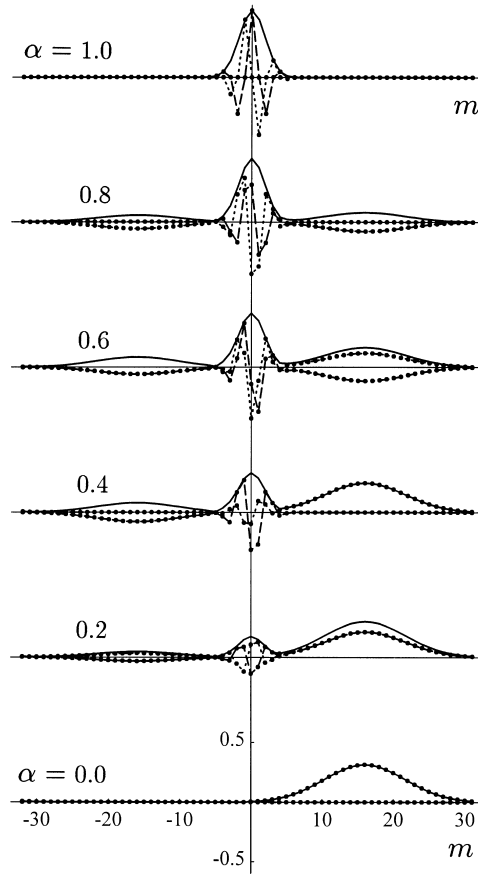


Fig. 3. Gaussian function under the finite fractional Fourier-exponential transform by powers (from bottom to top) $\alpha = 0, 0.2, \dots, 1$. There are $M = 64 = 2^6$ points on the horizontal axis $m = -32, -31, \dots, 31$. The real and imaginary parts of the vector components are marked \bullet , and joined by lines: --- and \dots respectively; the continuous line indicates the modulus. Compare with Fig. 2.

3. Fractional Fourier–Kravchuk transform

The search for a finite orthonormal basis of vectors $\{\Phi_n\}_{n=0}^N$, where the fractional Fourier transform matrix is the exponential generated by the diagonal *number* matrix $N = \text{diag}(0, 1, \dots, N)$,

$$D^\alpha = \exp(-i\frac{1}{2}\pi\alpha N) = \text{diag}(1, e^{-i\frac{1}{2}\pi\alpha}, \dots, e^{-N i\frac{1}{2}\pi\alpha}), \quad (20)$$

can be seen in the same Lie-theoretic context as the Fourier integral transform embedded in the linear canonical transforms in Section 1. Since the dimension of the vector space of data sets is finite, we should propose the $(N + 1) \times (N + 1)$ unitary representation of a compact group that contains the one-parameter subgroup (20). As we now show, our solution is the group of 2×2 special unitary matrices $SU(2)$ in the representation of $\text{spin } \ell = \frac{1}{2}N$. This is a natural way to define the régime of *finite* optics as the discrete analogue of paraxial optics.

The Newton equation for a harmonic oscillator and the ray equation for a waveguide in the paraxial régime are of the form $\ddot{q} = -wq$. The quantization/wavization of this relation replaces the position q by an operator \underline{Q} represented by a matrix \mathbf{Q} , and derivatives by i times the commutator with a Hamiltonian operator H , represented by a matrix \mathbf{H} , namely

$$[\mathbf{H}, [\mathbf{H}, \mathbf{Q}]] = w\mathbf{Q}, \Rightarrow \begin{cases} [\mathbf{H}, \mathbf{Q}] = -i\mathbf{P}, & \text{(geometry)} \\ [\mathbf{H}, \mathbf{P}] = iw\mathbf{Q} & \text{(dynamics)}. \end{cases} \tag{21}$$

The last two commutators are the two Hamilton equations that factorize the Newton equation into a geometric definition of the *momentum* operator P through its representing matrix \mathbf{P} , and its dynamical equation. Nothing is said however, of the key commutator $[\mathbf{Q}, \mathbf{P}]$, that in a Lie algebra should represent $[Q, P]$. The operators H , Q , and P , can be the generators of a Lie algebra provided that the Jacobi identity holds (i.e., the double commutators among the cyclic permutations of the three generators add up to zero). Using (21), this requires the ‘missing’ commutator between position and momentum operators to satisfy

$$[\mathbf{H}, [\mathbf{Q}, \mathbf{P}]] = 0, \Rightarrow [\mathbf{Q}, \mathbf{P}] = \begin{cases} iA \text{ (center)} & \text{Osc, or} \\ -iH + i\beta A & U(2), \text{ or} \\ iH + i\gamma A & U(1, 1). \end{cases} \tag{22}$$

The first choice leads to the *oscillator* algebra and group, indicated Osc, which is generated by four operators: Q , P , H , and a A commuting with all others. This leads to the common treatment of the quantum mechanical oscillator, where the representing matrix A is a multiple $\hbar = h/2\pi$ of $\mathbf{1}$], or to the paraxial optical waveguide, where the multiplicative constant is the reduced wavelength, $\lambda/2\pi$ [set to unity in Eq. (9)]. The second or third choices lead, respectively, to the Lie algebras and groups $U(2)$ or $U(1, 1)$, of 2×2 unitary or pseudo-unitary matrices whose determinant is a complex number of unit modulus. When the dynamics in (21) is such that $w = 0$, the generated algebras and groups can be Osc, or the Euclidean or pseudo-Euclidean groups on the plane, $ISO(2)$ or $ISO(1, 1)$ [25].

Only the $U(2)$ case has finite unitary representation matrices of dimensions $2\ell + 1$, for $\ell = 0, \frac{1}{2}, 1, \dots$; the other cases are all infinite-dimensional or represented by integral transform kernels. The central algebra element A generates only (necessary) phases but is otherwise uninteresting; we shall thus consider mostly the other three, which generate the subgroup of unitary matrices with unit determinant, commonly denoted $SU(2)$. We freely use thus the well-known results of angular momentum theory in quantum mechanics, to relate the position and momentum observables with the $SU(2)$ generator matrices

$$\mathbf{J}_1 = \mathbf{Q}, \quad \mathbf{J}_2 = -\mathbf{P}, \quad \mathbf{J}_3 = \mathbf{H} - (\ell + \frac{1}{2})\mathbf{1}, \tag{23}$$

whose Lie algebra and Casimir operator are easily recognized to be

$$[\mathbf{J}_1, \mathbf{J}_2] = i\mathbf{J}_3, \quad [\mathbf{J}_2, \mathbf{J}_3] = i\mathbf{J}_1, \quad [\mathbf{J}_3, \mathbf{J}_1] = i\mathbf{J}_2, \tag{24}$$

$$\mathbf{J}^2 = \mathbf{J}_1^2 + \mathbf{J}_2^2 + \mathbf{J}_3^2 = \ell(\ell + 1)\mathbf{1}, \tag{25}$$

and determining the irreducible representation to be of spin ℓ . The index ℓ will be henceforth understood in the context, and suppressed in the notation for vectors and matrices.

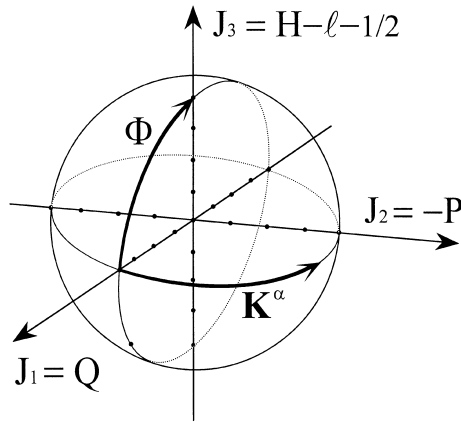


Fig. 4. Sphere of normalized SU(2) algebra generators: position $\mathbf{Q} = \mathbf{J}_1$, momentum $\mathbf{P} = -\mathbf{J}_2$ and mode/energy, $\mathbf{H} = \mathbf{J}_3 + (\ell + \frac{1}{2})\mathbf{1}$ of the finite oscillator; their eigenvalues are indicated on the axes. The Kravchuk transform Φ rotates the \mathbf{J}_1 axis by $\frac{1}{2}\pi$ onto the \mathbf{J}_3 axis. The fractional Fourier–Kravchuk transform \mathbf{K}^α rotates the sphere around the \mathbf{J}_3 axis by an angle $\frac{1}{2}\pi\alpha$, representing (but for a phase $\exp(i\frac{1}{4}\pi\alpha)$) the evolution of a wavefield along the axis of a shallow multimodal waveguide.

Among the elementary consequences of this correspondence is that the spectrum of any element of the SU(2) algebra, $J^{(\Omega)} = \sum_k u_k^{(\Omega)} J_k$ [normalized by $\sum_k u_k^{(\Omega)^2} = 1$, for $\Omega = (\theta, \phi)$ on the sphere], is the equally spaced set of $2\ell + 1$ points $m \in \{-\ell, -\ell + 1, \dots, \ell\}$. See Fig. 4. The Hamiltonian operator H has the nondegenerate spectrum of J_3 plus a constant: $n + \frac{1}{2} = \ell + m + \frac{1}{2} \in \{\frac{1}{2}, \frac{3}{2}, \dots, 2\ell + \frac{1}{2}\}$, so it defines an orthonormal basis. The vectors of this mode eigenbasis of \mathbf{J}_3 are labelled by m , and are $(2\ell + 1)$ -dimensional column vectors, that satisfy

$$\mathbf{J}_3 \mathbf{Z}_m = m \mathbf{Z}_m, \quad \mathbf{Z}_m = (\mathbf{Z}_m(m'))_{m'=-\ell}^{\ell}. \quad (26)$$

(In Dirac's notation the eigenvectors would be indicated by $|\ell, m\rangle_3$.) These represent the standing modes of the waveguide, which only evolve by a multiplicative phase,

$$\exp(-i\tau\mathbf{H}) \mathbf{Z}_m = \exp(-i\tau(\mathbf{J}_3 + (\ell + \frac{1}{2})\mathbf{1})) \mathbf{Z}_m = e^{-i\tau(m+\ell+\frac{1}{2})} \mathbf{Z}_m. \quad (27)$$

Thus we identify the finite oscillator, noting again that the Hamiltonian evolution (27) and the desired diagonal form of the Fourier transform (20) differ by a phase

$$\mathbf{D}^\alpha = \exp(-i\frac{1}{2}\pi\alpha(\mathbf{H} - \frac{1}{2}\mathbf{1})) = e^{i\pi\alpha/4} \exp(-i\frac{1}{2}\pi\alpha\mathbf{H}). \quad (28)$$

The matrices represent a one-parameter closed subgroup of $U(2)$, 2×2 unitary matrices (whose determinant can be a phase). In this basis, $\mathbf{D}^2 \mathbf{Z}_m = (-1)^{\ell+m} \mathbf{Z}_m$. As in the integral transform case, where waveguide evolution takes place in the metaplectic group (two-fold cover of the fractional Fourier transform cycle $\alpha \bmod 4$), waveguide evolution in the finite case also covers twice the fractional Fourier–Kravchuk transform cycle: for $\alpha = 4$ the evolution matrix $\exp(-i2\pi\mathbf{H}) = -\mathbf{1}$ is corrected by the sign $e^{i\pi} = -1$, so that $\mathbf{D}^4 = \mathbf{1}$. The fractional Fourier–Kravchuk transform matrices satisfy therefore the one-parameter subgroup composition property by construction, and are unitary.

It is important to note that in the finite oscillator/waveguide model, the spectra of both the position operator, $\mathbf{Q} = \mathbf{J}_1$ and the momentum operator $\mathbf{P} = -\mathbf{J}_2$, are also structurally discrete and finite. We

can write the eigenbasis of the position operator as the $(2\ell + 1)$ -dimensional canonical column vectors,

$$J_1 X_m = m X_m, \quad X_m = (X_m(m'))_{m'=-\ell}^{\ell}, \quad X_m(m') = \delta_{m,m'}. \tag{29}$$

(These would be indicated $|\ell, m\rangle_1$ in Dirac’s notation.) This basis is orthonormal: $X_m^T X_{m'} = \delta_{m,m'}$; and complete: $\sum_m X_m X_m^T = \mathbf{1}$. If the field-sensing array across the waveguide registers the values f_m at the sensors numbered by m , the input vector will be $\mathbf{f} = \sum_m f_m X_m$.

Now, by means of a rotation of $-\frac{1}{2}\pi$ around the 2-axis we can bring the 1-axis onto the 3-axis, to express the Z_m vectors (26) of mode number $n = \ell + m \in \{0, 1, \dots, 2\ell\}$, in terms of the canonical position basis for signals X_m , (29), with sensor number $m \in \{-\ell, -\ell + 1, \dots, \ell\}$,

$$\begin{aligned} Z_m &= \sum_{m'} X_{m'} X_{m'}^T Z_m = \sum_{m'} X_{m'} X_{m'}^T e^{-i\pi/2 J_2} X_m \\ &= \sum_{m'} X_{m'} Z_{m'}^T e^{+i\pi/2 J_2} Z_m = \sum_{m'} X_{m'} d_{m',m}^{\ell}(\frac{1}{2}\pi), \end{aligned} \tag{30}$$

where $d_{m',m}^{\ell}(\frac{1}{2}\pi)$ are the ‘Wigner little- d ’ matrix elements. For any colatitude angle θ , they are defined in Ref. [9] [Eqs. (3.65)] as

$$\begin{aligned} d_{m,m'}^{\ell}(\theta) &= \sqrt{(\ell + m)! (\ell - m)! (\ell + m')! (\ell - m')!} \\ &\quad \times \sum_k \frac{(-1)^{m-m'+k} (\cos \frac{1}{2}\theta)^{2\ell+m'-m-2k} (\sin \frac{1}{2}\theta)^{m-m'+2k}}{(\ell + m' - k)! k! (m - m' + k)! (\ell - m - k)!} \\ &= (-1)^{m-m'} \sqrt{\frac{2^{2(\ell-m)} (\ell - m)! (\ell + m)!}{2^{2\ell} (\ell - m')! (\ell + m')!}} k_{\ell-m}^{(\sin^2 \frac{1}{2}\theta)}(\ell - m', 2\ell) \end{aligned} \tag{31}$$

(The last term writes the Wigner little d -functions in terms of nonsymmetric Kravchuk polynomials [13,17,26], $k_n^{(p)}(j, 2\ell)$, which is *not* given in Ref. [9].)

The rows of Z_m in the canonical sensor position basis $X_{m'}$ are $Z_m(m') = d_{m',m}^{\ell}(\frac{1}{2}\pi)$. While $m' \in \{-\ell, -\ell + 1, \dots, \ell\}$ numbers the sensor point, the mode number $n = \ell + m$ counts the finite oscillator/waveguide wavefunctions for $n \in \{0, 1, \dots, N\}$, $N = 2\ell$. To indicate this explicitly, we introduce the *Kravchuk functions* defined by

$$\Phi_n^{\ell}(m) = (-1)^{\ell-n} Z_{\ell-n}(m) = (-1)^{\ell-n} d_{m,\ell-n}^{\ell}(\frac{1}{2}\pi). \tag{32}$$

The Kravchuk functions [4,5] have the explicit form (supressing ℓ)

$$\Phi_n(m) = \frac{1}{2^{\ell-n}} \sqrt{\binom{2\ell}{\ell+m} / \binom{2\ell}{n}} k_n(\ell + m, 2\ell), \tag{33}$$

in terms of the *symmetric Kravchuk polynomials* [13,17,26],

$$k_n(n', 2\ell) = \frac{(-1)^n}{2^n} \binom{2\ell}{n} {}_2F_1(-n, -n'; -2\ell; 2). \tag{34}$$

In the limit $\ell \rightarrow \infty$, and for ever closer points $x = m/\sqrt{\ell}$, the Kravchuk functions on the integers converge to the values of the harmonic oscillator wavefunctions:

$$\lim_{\ell \rightarrow \infty} \Phi_n(x\sqrt{\ell}) \rightarrow \Psi_n(x). \tag{35}$$

These polynomials are real and orthogonal under the binomial weight function $2^{-2\ell} \binom{2\ell}{n'}$ over the set of points $n' = 0, 1, \dots, 2\ell$. This implies that the Kravchuk functions (33) are real and orthonormal with constant weight.

In Fig. 5 we show some of the finite oscillator mode eigenfunctions for $2\ell + 1 = 65$. For small n 's they closely resemble the well-known harmonic oscillator wavefunctions, while for middle and large values of n , they are increasingly different. In particular, the highest-‘energy’ eigenfunction $n = 2\ell$ has the envelope of the lowest one, only alternating the signs of neighboring points. Their parity is $\Phi_n(m) = (-1)^n \Phi_n(-m)$, which follows from the index symmetry of the little d 's. The Kravchuk functions (32) we place as rows of the Kravchuk eigenvectors Φ_n , and with these columns we build the *Kravchuk matrix*:

$$\Phi_n = (\Phi_n(m))_{m=-\ell}^{\ell}, \quad \Phi = (\Phi_0 \Phi_1 \dots \Phi_{2\ell}). \tag{36}$$

From (27), (28), and (20), it follows that

$$K^\alpha \Phi = \Phi D^\alpha \Rightarrow K^\alpha = \Phi D^\alpha \Phi^\top. \tag{37}$$

In particular $(K^2 \Phi_n)(m) = (-1)^n \Phi_n(m) = \Phi_n(-m)$, and therefore K^2 is the inversion matrix (in the basis of sensor points), and $K^4 = \mathbf{1}$.

A column vector f whose components in the ‘position basis’ are the readings of the $2\ell + 1$ sensors $\{f_m\}_{m=-\ell}^{\ell}$, in the number basis of modes will have components $\{f_n^K\}_{n=0}^N$, with $N = 2\ell$ and $n = \ell + m$:

$$\sum_{m=-\ell}^{\ell} f_m X_m = f = \sum_{n=0}^{2\ell} f_n^K \Phi_n. \tag{38}$$

The two vectors $f = (f_m)_{m=-\ell}^{\ell}$ and $f^K = (f_n^K)_{n=0}^{2\ell}$ will be connected by the Kravchuk matrix, which is real and orthogonal,

$$f^K = \Phi^\top f. \tag{39}$$

This is the action of the rightmost factor of the Fourier–Kravchuk matrix K^α in Eq. (37). Now that the signal has been Kravchuk-transformed to the mode basis by Φ^\top , the diagonal matrix D^α of (20) is applied, and the vector is inverse-Kravchuk-transformed to the predicted values of the $2\ell + 1$ sensors. The elements of the Fourier–Kravchuk matrix K^α (37) in the sensor basis can be calculated in closed form [6] as

$$\begin{aligned} K_{m,m'}^\alpha &= X_m^\top \exp(-i\frac{1}{2}\pi\alpha(J_3 + \ell)) X_{m'} = \sum_{n=0}^{2\ell} \Phi_n(m) e^{i n \pi \alpha / 2} \Phi_n(m') \\ &= e^{i\pi(m+m'-\ell)\alpha/2} \sqrt{\binom{2\ell}{\ell-m} \binom{2\ell}{\ell-m'}} \cos^{2\ell} \frac{1}{4} \pi \alpha \tan^{2\ell+m+m'} \frac{1}{4} \pi \alpha \\ &\quad \times {}_2F_1 \left(m - \ell, m' - \ell; -2\ell; \frac{1}{\sin^2 \frac{1}{4} \pi \alpha} \right). \end{aligned} \tag{40}$$

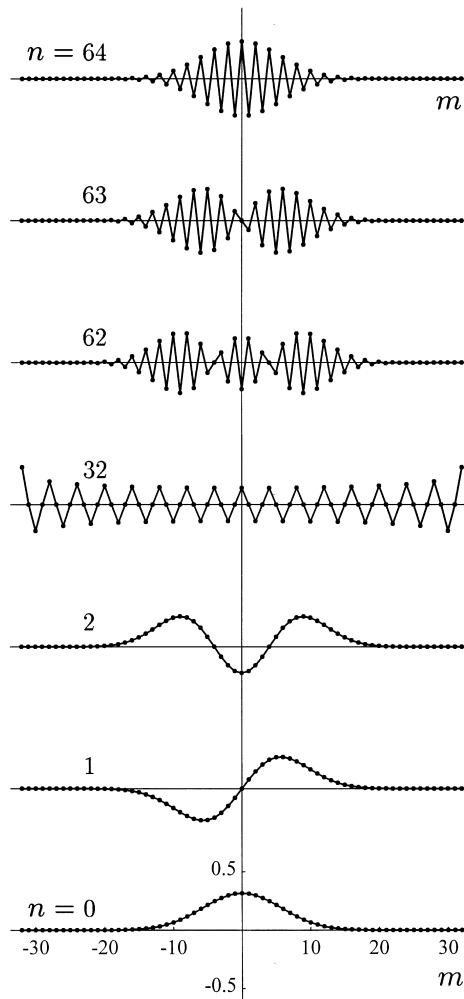


Fig. 5. Kravchuk eigenvectors $\Phi_n(m)$ for the finite oscillator of $2\ell + 1 = 65$ points (joined by straight lines). From bottom to top: the $n = 0$ ground state is the root of the binomial distribution; states $n = 1, 2, \dots, 32, \dots, 62, 63, 64$. The last is the highest-energy state that the waveguide can carry: it is the alternating root of the binomial distribution. Compare with the first few harmonic oscillator wavefunctions.

Although the fractional Fourier–Kravchuk matrix elements (40) have an explicit analytic expression that looks rather arduous to compute, we have calculated this transform easily using the matrix product form in Eq. (37). First, the *Kravchuk* transform (39) is performed: $\mathbf{f} \mapsto \mathbf{f}^K = \Phi^T \mathbf{f}$, using the Feinsilver–Schott algorithm [14] as detailed in the Appendix. Second, the components of the vector \mathbf{f}^K are multiplied by the elements of the diagonal matrix \mathbf{D}^α in (37). And third, the transpose Kravchuk transform Φ is applied to yield the fractional Fourier–Kravchuk transform vector $\mathbf{f}^{(\alpha)} = \mathbf{K}^\alpha \mathbf{f}$. The matrix \mathbf{K}^α thus generates the evolution of the field along a multimodal waveguide, sensed at $2\ell + 1$ points across the optical axis, at a distance which is $\frac{1}{4}\alpha$ of the guide period.

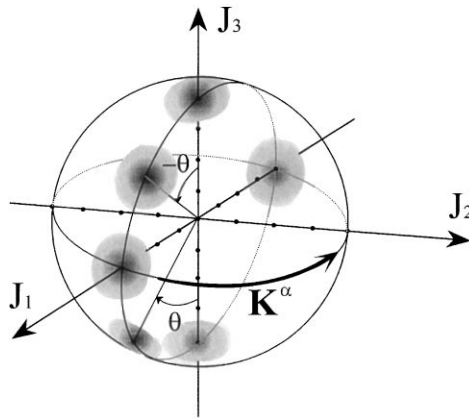


Fig. 6. Kravchuk coherent states on the sphere of normalized SU(2) algebra elements (cf. Fig. 4). The caps illustrate schematically the coherent states associated with extreme eigenvectors. The south cap is the finite oscillator ground state $Z_{-\ell}$, and the north cap the highest-energy state Z_{ℓ} . The caps on the J_1 direction are the two extreme localized states $X_{\pm\ell}$. By means of rotations one can bring the ground and highest coherent states to any other coherent or anti-coherent state on the same hemisphere (see the following figure). Evolution along the axis of the waveguide is their fractional Fourier–Kravchuk transform K^{α} .

4. Coherent states

From Eq. (32), the ground state of the $(2\ell + 1)$ -point finite oscillator is

$$\Phi_0(m) = d_{m,\ell}^{\ell}(\frac{1}{2}\pi) = \frac{1}{2^{\ell}} \sqrt{\binom{2\ell}{\ell+m}}. \quad (41)$$

It is a *coherent state* because it is the *extreme* normalized state among the eigenstates of J_3 (i.e., it is annihilated by the lowering operator $J_1 - iJ_2$ [4,5]). In the $\ell \rightarrow \infty$ limit (35), this binomial distribution converges to the well-known Gaussian oscillator ground state. In Fig. 6 we draw the ground state as a diffuse cap on the south pole of the sphere of Fig. 4, to indicate that it is a mode eigenstate (on the vertical axis of J_3) and a spread of values on the sensor basis (the horizontal axis $J_1 = Q$). From Eqs. (27) and (28), and as is clear from Fig. 6, the ground state (41) will be invariant under fractional Fourier–Kravchuk transforms, because these rotate the sphere around the 3-axis. Below we show the actual Kravchuk coherent state vectors.

Extreme states can be found for operators $J^{(\Omega)} = \sum_k u_k^{(\Omega)} J_k$, for every point $\Omega = (\theta, \phi)$ on the unit sphere. They can be obtained by means of rotations of the sphere of normalized operators in Fig. 4, and are shown in Fig. 6 as caps under different axes. The fact that these caps indeed represent coherent states can be understood through the Wigner function of the signal (in localized eigenstates of J_1), as shown in Ref. [3]. Rotations parametrized in Euler angles are generated by $R(\phi, \theta, \psi) = e^{i\phi J_3} e^{i\theta J_2} e^{i\psi J_3}$; the rightmost factor [a fractional Fourier–Kravchuk transform (28) for $\psi = \frac{1}{2}\pi\alpha$] acting on the ground state (41), will only multiply it by the constant phase $e^{-i\psi}$; the middle factor [a *fractional Kravchuk* transform – cf. Eqs. (30)] will be represented by the Wigner

little- d matrix,

$$(e^{i\theta/2} \mathbf{f})_m = \sum_{m'=-\ell}^{\ell} d_{m,m'}^{\ell}(\theta) f_{m'}; \tag{42}$$

finally, the leftmost factor [a fractional Fourier–Kravchuk transform for $\phi = \frac{1}{2}\pi\alpha$] yields the coherent state $\Phi_0^{(\Omega)}(m)$ labelled by $\Omega = (\theta, \phi)$. The ground state is given by (41); therefore, disregarding the phase $e^{-i\ell\psi}$, we can write coherent states in terms of the Wigner little d 's in (31)–(32) as

$$\Phi_0^{(\theta, \phi)}(m) = K^{2\phi/\pi} \sum_{m'=-\ell}^{\ell} d_{m,m'}^{\ell}(\theta) \Phi_0^{(0,0)}(m'). \tag{43}$$

But the remaining fractional Fourier–Kravchuk transform only corresponds to the phase ϕ of the coherent state oscillation along the waveguide. If we choose coherent states at their maximal amplitude (that start from rest at $\phi=0$), using (41) and the sum properties of the Wigner little- d 's, we can label the general coherent states (43) by the single colatitude angle θ of the operator $J_3 \cos \theta + J_1 \sin \theta$,

$$\Phi_0^{(\theta)}(m) = d_{m,\ell}^{\ell}(\theta + \frac{1}{2}\pi). \tag{44}$$

For $0 \leq \theta \leq \frac{1}{2}\pi$, the cap that represents the coherent state in Fig. 6 will have its center in the lower hemisphere.

Anti-coherent states are represented by caps in the upper hemisphere. Indeed, the highest mode $n = 2\ell$ in (32) is

$$\Phi_{2\ell}(m) = (-1)^{\ell} Z_{-\ell}(m) = (-1)^{\ell} d_{m,-\ell}^{\ell}(\frac{1}{2}\pi) = (-1)^{\ell-m} \Phi_0(m), \tag{45}$$

where we have used identities for the Wigner little- d functions [9, Eqs. (3.80)]; this state is represented by the cap on the north pole of Fig. 6. The anti-coherent signal states have the same envelope as the ground state, but neighboring points have opposite sign. For this state (45) we can repeat the rotations (42) to obtain the generic anti-coherent states

$$\Phi_{2\ell}^{(\theta)}(m) = d_{m,-\ell}^{\ell}(\theta + \frac{1}{2}\pi), \tag{46}$$

also for $0 \leq \theta \leq \frac{1}{2}\pi$. The caps that represent anti-coherent states have their center in the upper hemisphere. Where both hemispheres meet (say, along the $J_1 = Q$ axis at $\theta = \frac{1}{2}\pi$), the coherent/anticoherent states are $(0, \dots, 0, 1)$ or $(1, 0, \dots, 0)$. The Kravchuk coherent-state vectors for the caps of Fig. 6 are shown in Fig. 7. Rotation around the momentum axis by θ displaces the center of the ground-state bell, which unitarily narrows until it becomes an extreme localized state at $\theta = \frac{1}{2}\pi$. We can reach this same through displacing the highest-energy (anti-coherent) state by $-\theta$.

Fractional Fourier–Kravchuk transforms of finite-oscillator Kravchuk coherent states are shown in Figs. 8 and 9 for $\ell = 3$ and $\ell = 32$ respectively, i.e., for 7 and 65 points, and over a quarter-cycle. The latter are indistinguishable to the eye from that of the fractional Fourier integral transform of a Gaussian with the same center and width (by second moment), as that shown in Fig. 2. We believe that the correct description of coherent state evolution is a *sine qua non* condition for any discrete fractional Fourier transform. The Fourier–Kravchuk transform appears to have other interesting properties, which can be explored graphically. For example, the propagation of a localized state (a light pulse at a single point in the array) $X_m(m') = (0, \dots, 0, 1, 0, \dots, 0)$, both along and across the shallow waveguide is given by $K_{m,m'}^{\alpha}$ in (40) and shown first in Fig. 10. The fractional Fourier–Kravchuk transform of this pulse broadens showing a steep leading edge, as if it were a finite propagation velocity.

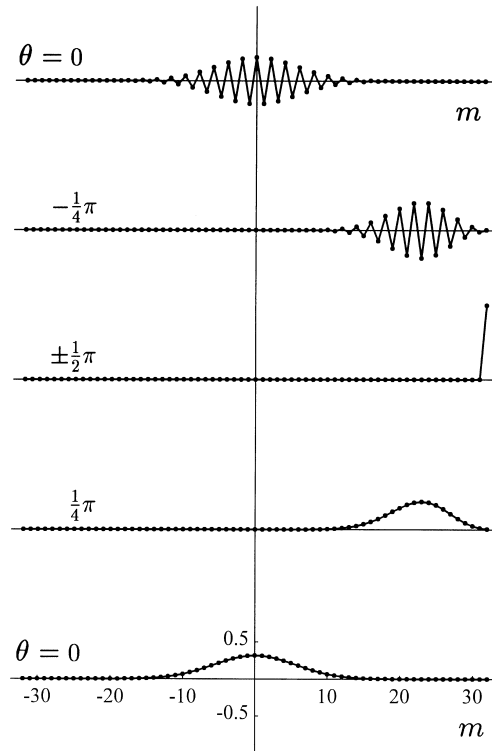


Fig. 7. Kravchuk coherent states $\Phi_{2\ell}^{(\theta)}(m)$ for $\ell = 32$ (65 points). At the bottom is the coherent ground state ($\theta = 0$), following up are the $\theta = \frac{1}{4}\pi$ and $\theta = \frac{1}{2}\pi$ coherent states. On top is the anti-coherent highest-energy state ($\theta = 0$), and following down its $-\theta$ -displaced states down to the extreme-localized (and coherent) state in the middle.

5. Discretization and fractionalization

Signal analysis is increasingly performed by miniaturized optical means. It is therefore relevant to study the discrete, finite versions of certain well-known mathematical operations, such as the Fourier and other ‘continuous’ integral transforms. The Fast Fourier Transform algorithm [10] is an excellent example of a computationally efficient tool for time-series analysis of signals in a homogeneous (or time-invariant) medium.

The optical counterpart of the Fourier transformation occurs between the two focal points of a lens, or at the end of a length of multimode graded-index waveguide. In particular, the refractive index of the waveguide must have a profile of negative curvature, like an (inverted) harmonic oscillator. But, because doped-chip waveguides are shallow, we should recognize that no more than a small number of transverse modes can be carried, and hence place not more than that number of field sensors across the guide. Such an optical model (Fig. 1) we consider discrete and finite. The finite Fourier (-exponential) transform counts its indices modulo M , as if sensors 1 and M were first neighbors. For Fourier–Kravchuk transforms on the other hand, sensor numbers 0 and N are literally poles apart. Waveforms moving (i.e., oscillating) toward an edge of the waveguide should pile up and reflect, as the state of Fig. 10, and not at all as Fig. 3, nor simply move through the

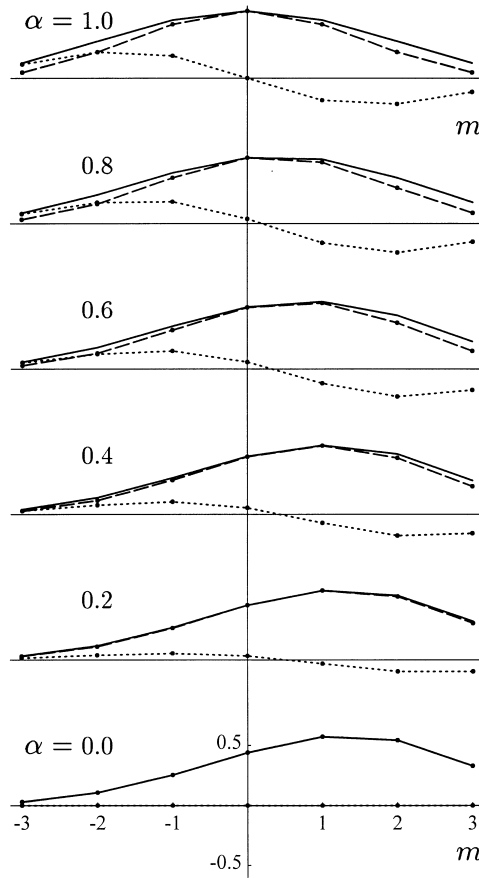


Fig. 8. Finite-oscillator Kravchuk coherent state of $\ell = 3$ (7 points), under fractional Fourier–Kravchuk transformation by powers (from bottom to top) $\alpha = 0, 0.2, \dots, 1$. The real and imaginary parts of the vector components are marked \bullet , and joined by lines: --- and $\dots\dots$ respectively; the continuous line is the modulus.

boundary reappearing on the opposite side, as time-series Fourier analysis could assume. For these reasons, we believe that propagation phenomena in multimodal waveguides are discretized best as Fourier–Kravchuk transforms.

Fractionalization of integral transforms is the second venue where optical applications have spurred interest. With optical arrangements, fractional Fourier transforms are performed as easily as the whole ones. They are naturally embedded as canonical transforms [22,23], within the *Weyl-symplectic group* $WSp(2, \mathfrak{R})$ [33, Chapter 10]. This group contains the linear symplectic transformations $Sp(2, \mathfrak{R})$, and also the Heisenberg–Weyl translations of phase space, and a multiplicative phase; the last three and the oscillator Hamiltonian generate the Osc group. Instead of Osc, however, the *finite optics model* adopts them with the deformed structure of the Lie algebra $U(2)$; one of the $\ell \rightarrow \infty$ contractions of $U(2)$ brings us back to Osc [30].

The subgroup of $U(2)$ generated by $J_3 + \ell$ is the Fourier transform cycle and, as we noted, rotates the sphere of Figs. 4 and 6 around the 3-axis. Similarly, the subgroup generated by $J_1 = Q$ rotates

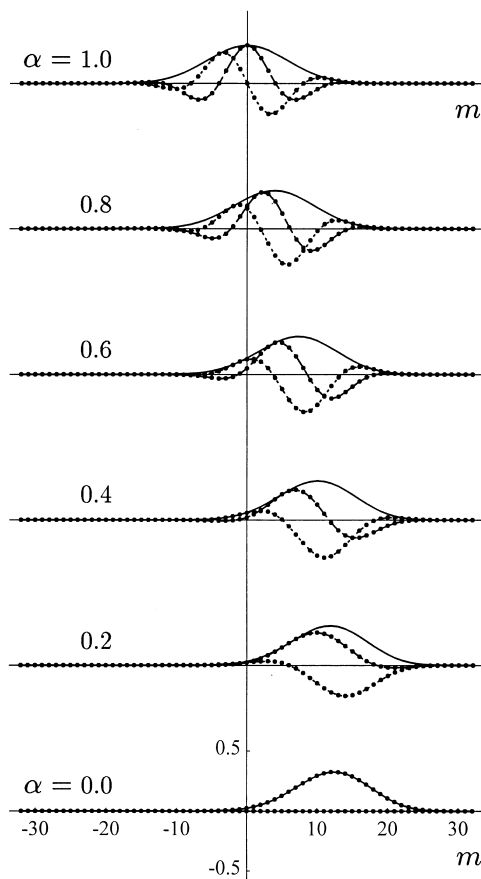


Fig. 9. Finite-oscillator Kravchuk coherent state of $\ell = 32$ (65 points) under fractional Fourier–Kravchuk transformation. All marks are as in the previous figure. Compare with the fractional Fourier integral transform of a true Gaussian in Fig. 2.

that sphere around the 1-axis, while multiplying the signal components by phases: $f_m \mapsto e^{im\beta} f_m$. Optically, this is realized by thin prisms of angle $\sim \beta$ within the waveguide that (in geometric optics and for small β) shift ray directions. These prisms produce unitary ‘translations’ of finite momentum space. Two prisms with opposite apices, i.e. an inclined slab within the guide, will translate positions, and realize the subgroup $\exp(i\gamma J_2)$. In Fig. 11 we show schematically the most general discrete optical system embedded in a waveguide that is ‘linear’ in $U(2)$, in the sense that its generators belong to the Lie algebra. Embedded lenses would multiply the signal components by quadratic phases $e^{im^2\chi}$ that are generated by the operators in the enveloping algebra of $U(2)$.

It is a recognized fact that difference equations have a richer solution set than their ‘continuous limit’ differential equations. As the number of points increases (with the intervals decreasing appropriately), both Fourier–Kravchuk and Fourier-exponential finite transforms become the Fourier integral transform in the limit [6,10]; but their fractionalizations (as studied here) are inequivalent. We have found it advantageous to embed the operation to be fractionalized within a multiparameter

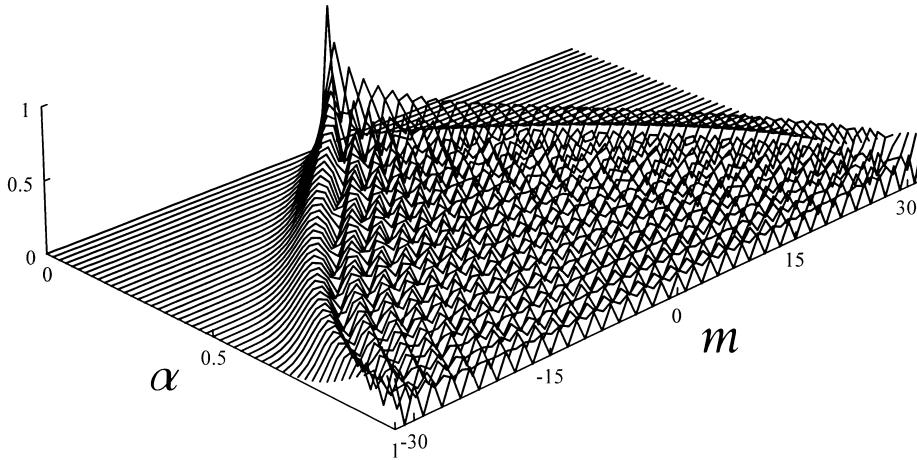


Fig. 10. A pulse $X_0(m) = (0, \dots, 0, 1, 0, \dots, 0)$ at the center of a waveguide propagates along α according to the fractional Fourier–Kravchuk transform K^α for 65 points ($|m| \leq 32$). The modulus of the wavefield is shown within a quarter-cycle length of waveguide, $0 \leq \alpha \leq 1$.

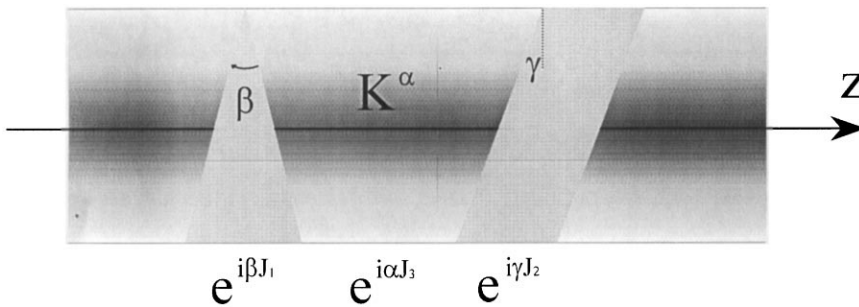


Fig. 11. The most general $SU(2)$ discrete optical system is composed of waveguide lengths (fractional Fourier–Kravchuk transform), prisms (multiplication of field values by a linear set of phases), and inclined slabs (unitary translation of discrete positions).

Lie group of transformations. Finally, we have seen that numerical simulations are useful for understanding the computational efficiency of the Feinsilver–Schott algorithm given in the Appendix.

Acknowledgements

This work was performed with the support of Project DGAPA-UNAM IN104198 ‘Optica Matemática’. One of us (LEV) acknowledges the Consejo Nacional de Ciencia y Tecnología for an assistant scholarship. We thank Dra. Ana Leonor Rivera for discussions on this work, and the indispensable help of Quím. Guillermo Krötzsch with the figures.

Appendix. The Feinsilver–Schott algorithm

In Ref. [14], Feinsilver and Schott discovered an algorithm which, by sums and differences, transforms an input $(N + 1)$ -component set of values $v = \{v_n\}_{n=0}^N$ into a set $\tilde{v}^k = \{\tilde{v}_n^k\}_{n=0}^N$, of their expansion coefficients in Kravchuk polynomials. Since we use the Kravchuk functions (33) in expansion (38), normalization factors will have to be applied to both sets at the end.

The Feinsilver–Schott algorithm starts at step 0 by writing out a $1 \times (N + 1)$ array with the input data:

$$\begin{bmatrix} v_0 & v_1 & v_2 & \cdots & v_N \end{bmatrix}^0.$$

The first step creates a $2 \times N$ array of elements indicated by

$$\begin{bmatrix} v_n^v \end{bmatrix}^1,$$

whose first row $v=0$ sums contiguous entries, and whose second row $v=1$ contains their differences:

$$\begin{bmatrix} v_0^0 & v_1^0 & v_2^0 & \cdots & v_{N-1}^0 \\ v_0^1 & v_1^1 & v_2^1 & \cdots & v_{N-1}^1 \end{bmatrix}^1 = \begin{bmatrix} v_0 + v_1 & v_1 + v_2 & v_2 + v_3 & \cdots & v_{N-1} + v_N \\ v_0 - v_1 & v_1 - v_2 & v_2 - v_3 & \cdots & v_{N-1} - v_N \end{bmatrix}^0.$$

Repeating the process of summing contiguous row entries and adding a last row with difference, the m th step (indicated by the m on the array) creates, from the elements of the previous $m \times (N - m + 2)$ array, the $(m + 1) \times (N - m + 1)$ array

$$\begin{bmatrix} v_0^0 & v_1^0 & v_2^0 & \cdots & v_{N-m}^0 \\ v_0^1 & v_1^1 & v_2^1 & \cdots & v_{N-m}^1 \\ \vdots & \vdots & \vdots & & \vdots \\ v_0^{m-1} & v_1^{m-1} & v_2^{m-1} & \cdots & v_{N-m}^{m-1} \\ v_0^m & v_1^m & v_2^m & \cdots & v_{N-m}^m \end{bmatrix}^m = \begin{bmatrix} v_0^0 + v_1^0 & v_1^0 + v_2^0 & v_2^0 + v_3^0 & \cdots & v_{N-m-1}^0 + v_{N-m}^0 \\ v_0^1 + v_1^1 & v_1^1 + v_2^1 & v_2^1 + v_3^1 & \cdots & v_{N-m-1}^1 + v_{N-m}^1 \\ \vdots & \vdots & \vdots & & \vdots \\ v_0^{m-1} + v_1^{m-1} & v_1^{m-1} + v_2^{m-1} & v_2^{m-1} + v_3^{m-1} & \cdots & v_{N-m-1}^{m-1} + v_{N-m}^{m-1} \\ v_0^{m-1} - v_1^{m-1} & v_1^{m-1} - v_2^{m-1} & v_2^{m-1} - v_3^{m-1} & \cdots & v_{N-m-1}^{m-1} - v_{N-m}^{m-1} \end{bmatrix}^{m-1}.$$

After N steps, one obtains the $(N + 1) \times 1$ array

$$\begin{pmatrix} v_0^N \\ v_1^N \\ v_2^N \\ \vdots \\ v_N^N \end{pmatrix} = \begin{pmatrix} \tilde{v}_0^K \\ \tilde{v}_1^K \\ \tilde{v}_2^K \\ \vdots \\ \tilde{v}_N^K \end{pmatrix},$$

where in particular

$$\tilde{v}_0^K = \sum_{n=0}^N \binom{N}{n} v_n, \quad \tilde{v}_N^K = \sum_{n=0}^N (-1)^n \binom{N}{n} v_n,$$

are the binomial and alternating binomial distributions. If the resulting column array is transposed to a row and the above algorithm is repeated, it reproduces the previous steps backwards, but for a factor of 2 at each step. The Feinsilver–Schott algorithm applied twice thus reproduces the original data set with a factor of 2^N .

Because the Kravchuk functions in our expansion (38) and the Kravchuk polynomials are related by (33) with a ratio of binomial coefficients, the *Kravchuk transform* of $\mathbf{f} = \{f_m\}_{m=-\ell}^{\ell}$ can be obtained in three steps. First we renumber the components according to $n = \ell + m \in \{0, 1, \dots, 2\ell\}$, multiplying the components by a diagonal matrix,

$$\mathbf{v} = \text{diag}(\sqrt{(2\ell - n)! n!}) \mathbf{f}. \tag{47}$$

Second, using the Feinsilver–Schott algorithm on \mathbf{v} we produce $\tilde{\mathbf{v}}^K$ as described above. And third, we multiply the result by a second diagonal matrix,

$$\mathbf{f}^K = 2^{-\ell} \text{diag} \left(\frac{(-1)^n}{\sqrt{(2\ell - n)! n!}} \right) \tilde{\mathbf{v}}^K. \tag{48}$$

This yields \mathbf{f}^K in (39).

It is a sobering fact that the Feinsilver–Schott algorithm for the Kravchuk transform is not a *fast* algorithm, as the FFT is [10]. Provided the Kravchuk transform matrix of given dimension $N + 1$ is known and stored, we recall that its application on the data vector requires $(N + 1)^2$ products and N^2 sums – a total of $\sim 2N^2$ operations. The Feinsilver–Schott algorithm performs, at step m , one sum or difference for each of the entries of the resulting $(m + 1) \times (N - m + 1)$ array. The number of operations is thus

$$\sum_{m=1}^N (m + 1)(N - m + 1) = \frac{1}{6}N(N + 1)(N + 5) \sim \frac{1}{6}N^3.$$

Yet not all advantage is lost: for small N , the algorithm is faster than matrix multiplication up to 7, i.e., for 8 data points; besides, the simplicity of the algorithm allows the design of a microchip circuit to perform Kravchuk transforms.

References

- [1] D. Achilles, On certain eigenstructure properties of discrete Fourier transforms and their applications to matched filtering, *Arch. Elektron. Übertragungstechnik* 42 (1988) 21–24.
- [2] G.S. Agarwal, R. Simon, A simple realization of fractional Fourier transform and relation to harmonic oscillator Green's function, *Opt. Commun.* 110 (1994) 23–26.
- [3] N.M. Atakishiyev, S.M. Chumakov, K.B. Wolf, Wigner distribution function for finite systems, *J. Math. Phys.* 39 (1988) 6247–6261.
- [4] N.M. Atakishiyev, S.K. Suslov, Difference analogs of the harmonic oscillator, *Teor. Math. Phys.* 85 (1991) 1055–1062.
- [5] N.M. Atakishiyev, K.B. Wolf, Approximation on a finite set of points through Kravchuk functions, *Rev. Mex. Fis.* 40 (1994) 366–377.
- [6] N.M. Atakishiyev, K.B. Wolf, Fractional Fourier–Kravchuk transform, *J. Opt. Soc. Amer. A* 14 (1997) 1467–1477.
- [7] C. Belingeri, P.E. Ricci, Una proprietà di una classe di trasformazioni integrali che generalizza la Transformata di Fourier, *Rend. Mat. S. VII* 14 1994.
- [8] C. Belingeri, P.E. Ricci, A generalization of the discrete Fourier transform, *Integr. Transforms Special Functions* 3 (1995) 165–174.
- [9] L.C. Biedenharn, J.D. Louck, *Angular Momentum in Quantum Physics Encyclopedia of Mathematics and its Applications*, vol. 8, Addison-Wesley, Reading, MA, 1981.
- [10] E.O. Brigham, *The Fast Fourier Transform*, Prentice-Hall, Englewood Cliffs, NJ, 1974.
- [11] E.U. Condon, Immersion of the Fourier transform in a continuous group of functional transformations, *Proc. Natl. Acad. Sci.* 23 (1937) 158–164.
- [12] B.W. Dickinson, K. Stieglitz, An approach to the diagonalization of the discrete Fourier transform, *IEEE Trans. ASSP* 30 (1982) 25–31.
- [13] A. Erdélyi, W. Magnus, F. Oberhettinger, F.G. Tricomi, *Higher Transcendental Functions*, vol. 2, McGraw-Hill, New York, 1953.
- [14] P. Feinsilver, R. Schott, Operator calculus approach to orthogonal polynomial expansions, *J. Comput. Appl. Math.* 66 (1996) 185–199.
- [15] F.A. Grünbaum, The eigenvectors of the discrete Fourier transform: A version of the Hermite functions, *J. Math. Anal. Appl.* 88 (1982) 355–363.
- [16] T. Hakioglu, Finite-dimensional Schwinger basis, deformed symmetries, Wigner function, and an algebraic approach to quantum phase, *J. Phys. A* 31 (1998) 6975–6994.
- [17] M. Krawtchouk, Sur une généralization des polinômes d'Hermite, *C.R. Acad. Sci. Paris* 189 (1929) 620–622.
- [18] J.H. McClellan, Comments on eigenvector and eigenvalue decomposition of the discrete Fourier transform, *IEEE Trans. AU* 21 (1973) 65.
- [19] J.H. McClellan, T.W. Parks, Eigenvalue and eigenvector decomposition of the discrete Fourier transform, *IEEE Trans. AU* 20 (1972) 66–74.
- [20] M.L. Mehta, Eigenvalues and eigenvectors of the finite Fourier transform, *J. Math. Phys.* 28 (1987) 781–785.
- [21] D. Mendlovic, Y. Bitran, R.G. Dorsch, A.W. Lohmann, Optical fractional correlation: experimental results, *J. Opt. Soc. Am.* 12 (1995) 1665–1670.
- [22] M. Moshinsky, C. Quesne, Linear canonical transformations and their unitary representations, *J. Math. Phys.* 12 (1971) 1772–1780.
- [23] M. Moshinsky, C. Quesne, Canonical transformations and matrix elements, *J. Math. Phys.* 12 (1971) 1780–1783.
- [24] V. Namias, The fractional order Fourier transform and its application to quantum mechanics, *J. Inst. Math. Appl.* 25 (1980) 241–265.
- [25] L.M. Nieto, N.M. Atakishiyev, S.M. Chumakov, K.B. Wolf, Wigner distribution function for Euclidean systems, *J. Phy. A* 31 (1998) 3875–3895.
- [26] A.F. Nikiforov, S.K. Suslov, V.B. Uvarov, *Classical Orthogonal Polynomials of a Discrete Variable*, Springer, Berlin, 1991.
- [27] H.M. Ozaktas, D. Mendlovic, Fractional Fourier optics, *J. Opt. Soc. Amer.* 12 (1995) 743–751.

- [28] T.S. Santhanam, Finite-space quantum mechanics and Krawtchuk functions, in: K. Srinivasa Rao, R. Jagannathan, J. Van der Jeugt, G. Van der Berghe (Eds.), *Proceedings of the Workshop on Special Functions and Differential Equations*, Allied Publishers Delhi, 1998.
- [29] T.S. Santhanam, A.R. Tekumalla, Quantum mechanics in finite dimensions, *Found. Phys.* 6 (1976) 583–589.
- [30] J.D. Talman, *Special Functions – A Group theoretic Approach*, W.A. Benjamin, New York, 1968 (Chapter 13).
- [31] R. Tolimeri, The construction of orthonormal bases diagonalizing the discrete Fourier transform, *Adv. Appl. Math.* 5 (1984) 56–86.
- [32] N. Wiener, *The Fourier Integral and Certain of its Applications*, Cambridge University Press, Cambridge, 1933.
- [33] K.B. Wolf, *Integral Transforms in Science and Engineering*, Plenum Publ. Corp., New York, 1979.
- [34] R. Yarlagadda, A note on the eigenvectors of DFT matrices, *IEEE Trans. ASSP* 25 (1977) 586–589.